LA-UR-08-6415

Approved for public release; distribution is unlimited.

Title:	Simulation of the Cygnus Rod-Pinch Diode Using the Radiographic Chain Model
Author(s):	Thomas J. T. Kwan Tai-Sen Wang Michael Berninger Charles M. Snell Lin Yin
Intended for:	IEEE Transactions on Plasma Science

Form 836 (7/06)

Simulation of the Cygnus Rod-Pinch Diode Using the Radiographic Chain Model

Thomas J. T. Kwan [a], Tai-Sen Wang [a], Michael Berninger [b], Charles Snell [a], Lin Yin [a]

[a] *Applied Physics Division, Los Alamos National Laboratory*
Los Alamos, NM 87545
505-667-3447, tjtk@lanl.gov

[b] *National Security Technologies, LLC, Los Alamos Operations*
182 East Gate Drive, Los Alamos, NM 87544

The Cygnus radiographic machine is a relatively compact low-energy (<3 MV) x-ray source with some extremely desirable features for radiographic applications. These features include small spot size critical for high-spatial resolution and high dose in a low energy range. The x-ray source is based on bremsstrahlung production in a small diameter (~0.75 mm) tungsten rod by a high-current (~60 kA) electron beam converging at the tip of the rod. For quantitative analysis of radiographic data, it is essential to determine the bremsstrahlung spectrum accurately. We have used the radiographic chain model that self-consistently models the diode with a two-dimensional particle-in-cell code (Merlin) which links to an electron-photon Monte Carlo code to obtain the spectrum under three different situations. These are: steady state spectrum using a voltage pulse of 2.5 MV, time-integrated spectrum using a time-dependent experimental voltage pulse, and inclusion of reflexing electrons at the anode in our particle-in-cell simulation. Detailed electron dynamics have been obtained in our study. Our investigations conclude that the time integrated bremsstrahlung spectrum is significantly softer than that of the steady state. In our latest simulations, we have included the effects of reflexing electrons around the anode rod and found the spectrum to be in better agreement with experimental data.

***Index Terms*- Cygnus, flash radiography, simulation, diode**

I. Introduction

Cygnus is an intense bremsstrahlung flash X-ray source that contains a rod-pinch diode[1] and associated pulsed power driver.[2] Used for radiography at the Nevada Test site, Cygnus demonstrates much-improved performance over alternative radiographic sources, due to dramatically reduced spot size (~ 1.1 mm related to the rod size) and a relatively large dose (> 4 rad @ 1m).[1] Although Cygnus produces high quality radiography, the diode physics and the resulting Bremsstrahlung spectrum have not been fully investigated and characterized, and quantitative radiography cannot be conducted to the desired precision.

A self-consistent simulation of the Cygnus diode and its generation of Bremsstrahlung photons have been performed with the radiographic chain model (RCM).[3] The RCM (Fig. 1) consists of the linked electromagnetic particle-in-cell (PIC) code Merlin[4], hydrodynamic code for evolution of the convert target, and the Monte Carlo Neutral Particle (MCNP) electron-photon transport code.[5] For the Cygnus source simulation, the hydrodynamic expansion of the rod is ignored due to consideration of the expected hydrodynamic time scale. PIC techniques provide an electromagnetically self-consistent simulation of the process of generation of electrons in the diode. Detailed distributions of the electron momenta and positions are obtained at the surface of the anode rod. The distributions are subsequently used in MCNP to model the electron transport in the anode rod. The electromagnetic fields are ignored inside the anode rod due to its high conductivity. The Bremsstrahlung process from the electron transport results in the radiographic photon spectrum from the Cygnus diode. With this high fidelity source simulation, the MCNP code could, in principle, calculate the photon transport in a 3-dimensional model of an experiment accurately for comparison with available data.

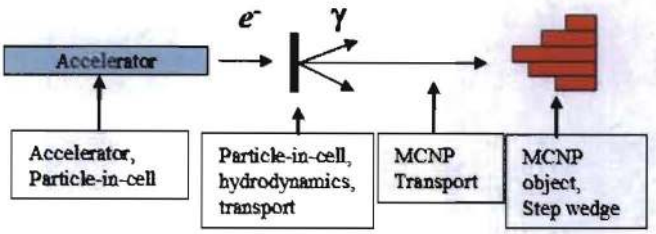

Figure 1. A schematic of the linked radiographic chain model.

The Cygnus calculations with Merlin were adapted in three stages where the complexity of the diode model was increased at each stage to better investigate the effects on overall fidelity of the model. In the first case, under the assumption that the peak voltage dominated the diode's radiographic performance, the current-voltage characteristic in the Cygnus model was approximated with a steady state voltage after a short rise time. The peak voltage of a typical Cygnus pulse was 2.5 MV. A "steady-state" x-ray spectrum was then calculated. In the second case, the current-voltage characteristic was modeled by using the measured Cygnus voltage pulse and a time-integrated spectrum was calculated. Last, the effects of electrons reflexing around the anode were investigated. In this situation, an electron that collides with the anode but retains enough of its kinetic energy can turn around and make multiple passes through the anode – or reflexing – generating lower energy

bremsstrahlung with each pass. This process of reflexing of electrons was modeled with the Monte Carlo technique in the Merlin PIC simulation[4], and the resulting spectrum was calculated.

This paper presents the results of the RCM investigations of the three simulation cases. X-ray bremsstrahlung transmissions were also calculated with a detailed step-wedge model in MCNP and analyzed. To validate the source models, these results were compared with step-wedge measurements made with Cygnus.

II. Radiographic Chain Model of Cygnus

A. Cygnus Diode Configuration

In the Cygnus design (Fig. 2), a rod-pinch diode[6,7] is enclosed in a chamber that has a typical vacuum of $1x10^{-5}$ torr. The diode is azimuthally symmetric consisting of a tungsten anode rod inserted through a 9 mm diameter hole in the center of the cathode, which is an annular aluminum disc. The tip of the anode rod can either be blunt or tapered and extends 1-cm beyond the cathode.

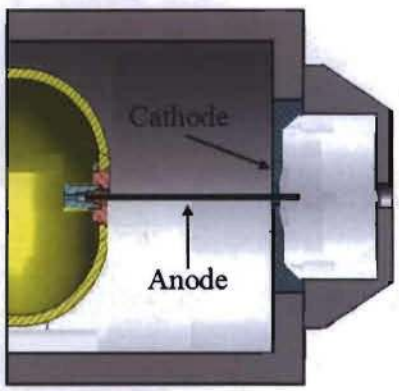

Figure 2. Cross sectional drawing of the Cygnus source.

The physics and operation principles of the rod-pinch diode were described by Cooperstein et. al[6,8] and references therein. We will only focus on simulation methodolgy and results of the Cygnus rod-pinch diode and Its bremsstrahlung spectra in the following sections.

B. Particle-in-cell Simulation of the Cygnus Diode

We have used the PIC code Merlin to simulate the electron beam dynamics in the rod-pinch diode in a self-consistent manner.[8] Merlin is a finite-difference, time-domain, two-dimensional (cylindrical symmetry in our calculations), fully electromagnetic, and relativistic PIC simulation code. From the PIC simulations, we obtained the spatial distribution functions (r and z) and momentum distributions (p_z, p_x, and p_y) of the electrons impinging on the anode rod.

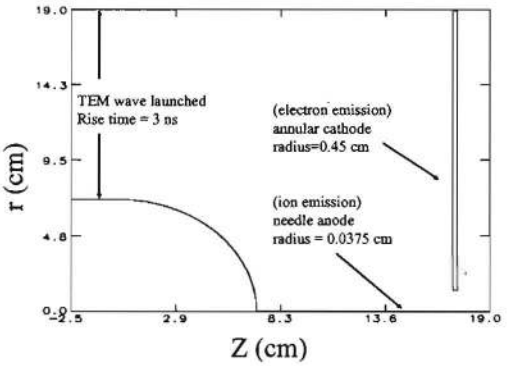

Figure 3. Geometry of the rod-pinch diode in PIC simulations.

Following the dimensions/parameters used in the Cygnus experiments, a 0.75-mm-diameter anode rod and a 9-mm-diameter aperture cathode were modeled in our simulations as shown in Fig. 3. The aspect ratio (ratio of the cathode-to-anode radius) is 12. In the 2D azimuthally symmetric geometry of the simulation, the curved surface at the bottom left corner of Fig. 3 is the anode stalk, which is connected to the anode rod centered around the z axis.

A space-charge-limited emission model is used for the generation of electrons and ions. In this model, the electric field threshold for electron (ion) emission is set to 50 kV/cm (100 kV/cm). The emitted particles initially have zero momentum. To shorten computing time, the ions are assumed to be hydrogen (with real mass ratio $m_i/m_e = 1836$ where m_i is the mass of the ion and m_e is electron mass). Consistent with the physical diode, a TEM wave is launched at the left boundary of the simulation geometry to set up the voltage required for the electron emission from the cathode. The current of the electron beam rises as the voltage increases. During the rise, the electron flow is governed by the physics of space-charge limited flow as shown in the top panel of Figure 4. However, as the electron current increases,

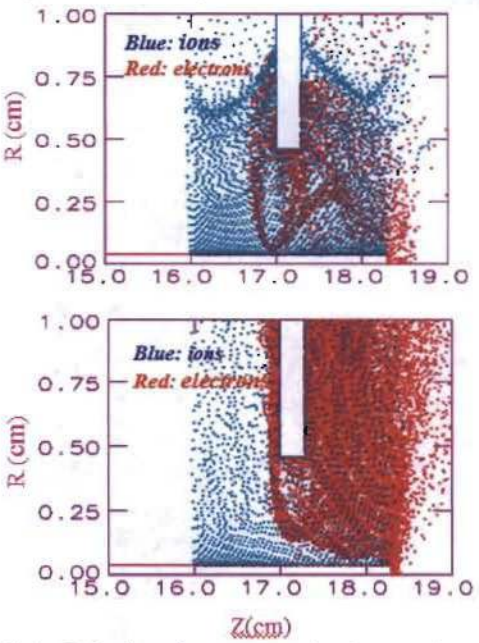

Fig.4: Early time electron dynamics (top panel) and later time electron dynamics (bottom panel).

the azimuthal magnetic field starts to strongly influence the electron trajectories. At the same time, plasma starts to form around the anode surface due to electron bombardments. The plasma significantly reduces the electric field near the anode. The magnetic force ($\vec{v} \times \vec{B}$ where $\vec{v}$ is velocity and $\vec{B}$ is the magnetic field) on the electrons eventually causes the electron flow to be magnetically dominated. When the voltage pulse has fully risen to 2.25 MV, the electron beam dynamics has changed from space-charge limited flow to magnetically insulated flow, in which the electrons drift along the anode surface until they finally converge at the tip of the anode rod. The descriptive name "rod-pinch" is attributed to this convergent phenomenon of the electron beam. The electron dynamics at this time is shown in the bottom panel of Fig. 4 from our PIC simulation. The physical behavior of a high current electron beam impinging on a small volume of bremsstrahlung converter produces an ideal point-source like x-ray radiographic source. The approximately spherical convergence of electrons into the tip of the tungsten rod generates a relatively isotropic bremsstrahlung source which does not have significant angular dependence.

C. *Three Simulation Cases*

Three sets of PIC simulations of the Cygnus diode were calculated in this study: the steady-state, the time integrated pulse, and Merlin Monte Carlo, which included the effects of electron collisions resulting in electron angular scattering and energy degradation within the anode in the steady state case. Each simulation case will be described in detail.

In the steady-state simulation, electron information was only collected after the driving electromagnetic pulse reached a final voltage plateau of 2.25 MV following a fast (~ 5 ns) rise time. Note that the electrons colliding with the diode during the rise and fall of the electromagnetic pulse are ignored. The electron distributions from our PIC simulation are shown in Fig. 5.

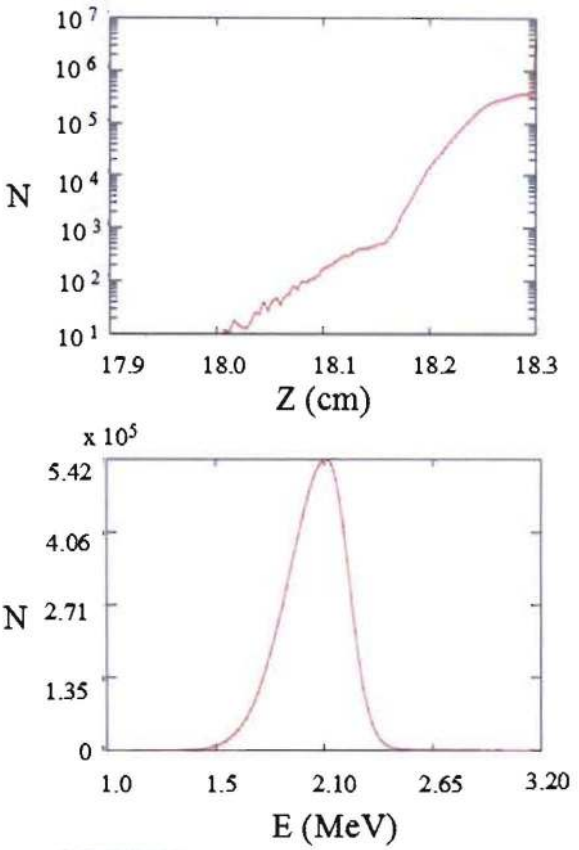

Figure 5. Distributions of electrons converging onto the tip of the tungsten rod in the steady state set of simulations.

The steady-state electron energy has a spread between ~1.5 MeV and 2.25 MeV with a peak at 2.1 MV. It is important to note that the electron distribution in z shows that most of the electrons converge to the tip of the anode rod. The electron dynamics exhibits the typical magnetically insulated flow along the anode rod leading to the eventual convergence at the tip of the anode rod.

We performed another PIC simulation of the Cygnus diode in which the experimentally measured diode current-voltage characteristic was modeled. The waveform in Fig. 6 (top panel) was a reference where the black curve is the diode voltage versus time whose amplitude rises to a peak value of ~2.3 MV. On average, the pulse lasted ~100 ns with a rise time of approximately 50 ns, a peak 20 ns long, and a 30 ns fall.

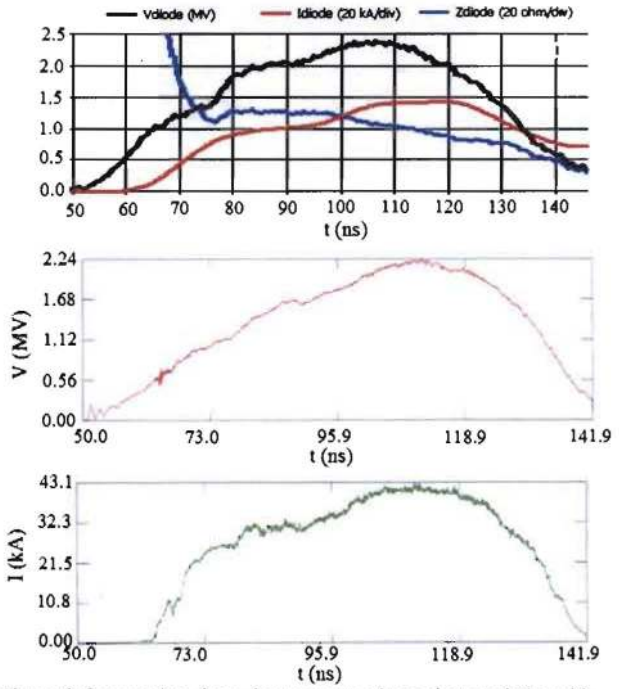

Figure 6. Cygnus time dependent current-voltage characteristics with impedance according to experimental data (top panel) and the corresponding voltage model used in the simulation (middle panel). The current was calculated (bottom panel).

Diode current as a function of time is the red curve. The current lags the voltage pulse by about 10 ns owing to the finite threshold of voltage for electron emission at the cathode surface. Near the end of the diode operation, the impedance (blue) exhibits collapse (i.e., toward zero value). Impedance collapse is expected as the gap between the cathode and the anode starts to close off electrically due to formation of plasmas.

In the diode simulation, the synthetic voltage pulse was input to the PIC code as shown in Fig 6 (middle panel) to model the dynamic transverse electromagnetic waveform (TEM). A current probe in the simulation monitored the current calculation shown in Fig 6. (bottom panel). The simulated current-pulse shape generally agrees with the measured current but its magnitude is ~30% lower than the measured pulse. This extensive PIC simulation was completed after about a month of continuous execution.

The positions and velocities of the electrons reaching the anode rod were recorded with three consecutive time intervals over the pulse period. During this period, the electron dynamics went through the stages from space-charge limited flow to magnetically insulated flow. The energy distribution and axial (z) distribution of the electrons at the three phases were constructed using time windows of 10 ns, 20 ns, and 10 ns at t = 77 ns (rise), 100 ns (peak), and 125 ns (fall) respectively. They are shown in Fig. 7.

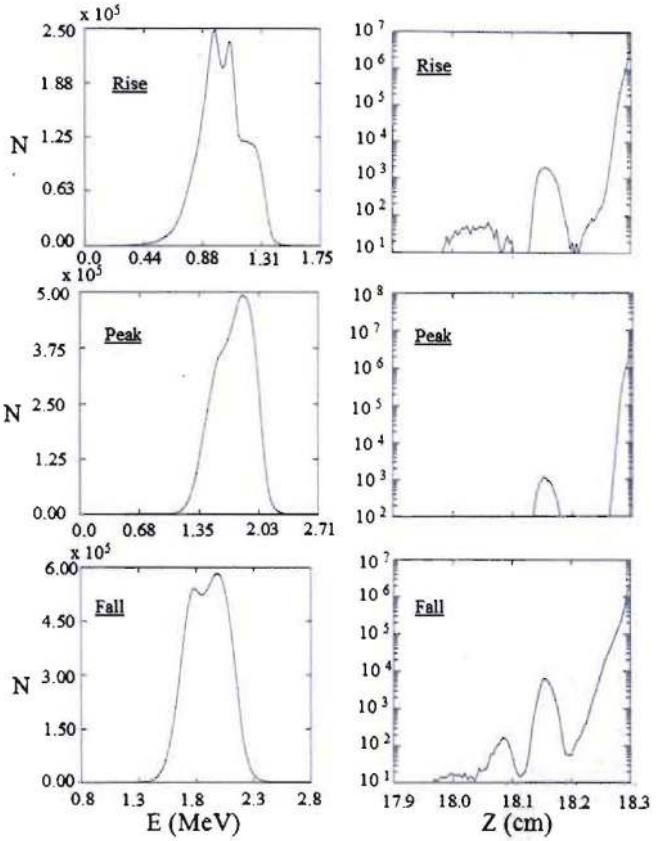

Figure 7. Electron distributions in Cygnus diode at three different time periods in the dynamical pulse simulations.

It is evident that at t = 77 ns the electrons have a mean energy about 1 MeV and they impinge on the rod over a fairly extended axial location. However, by the time the voltage pulse reaches its peak at t = 100 ns, the magnetically insulated flow already sets in, and the electrons move along the surface of the anode rod and eventually collapse at the tip with a mean energy of about 2 MeV. In the time period around 125 ns, the voltage pulse starts to fall. The energy distribution still peaks at an energy slightly greater than 2 MeV. However, the electron spatial distribution along the anode rod has a significant spread indicating that the dynamics of the electron flow has evidently changed to space-charge limited flow. The onset of this phenomenon is due to that the electron current has decreased to a level that self-magnetic insulation is no longer the dominant mechanism for the electron flow at this time. Consequently, the pinch dynamics diminishes.

Recent studies focus on improving the computational Cygnus spectra by using the Monte Carlo feature in Merlin to include the reflexed electrons around the anode rod. These resurfaced electrons can be turned around by the electric field between the cathode and the anode resulting in multiple passes by a single electron. Of course, the electron energy would be diminished as the electrons pass through the rod successively due to collision processes and bremsstrahlung production. For the re-try electrons, their contribution to the bremsstrahlung spectrum tend to be in the low energy region as their kinetic energy are gradually depleted. Figure 8 shows the energy

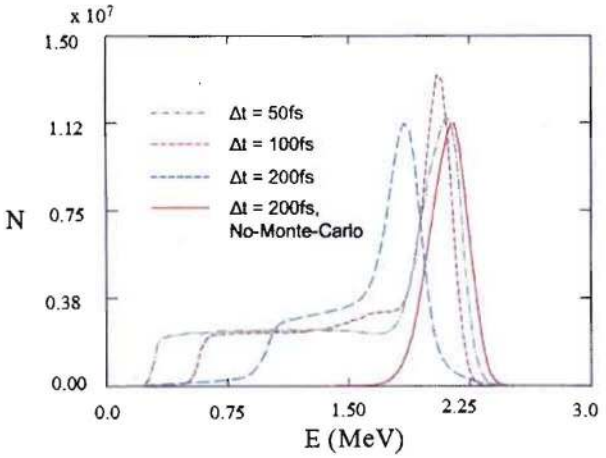

Figure 8. Electron distributions in Cygnus diode at three different time periods in the dynamical pulse simulations.

distributions of the electrons near the surface of the anode obtained from the calculation neglecting the reflexing electrons and from the calculations including the reflexing electrons for a few different time steps used in the simulations. Here, we see the low energy tail due to the reflexing electrons has a cut-off in energy depending on the time step used in the simulation. The relationship between the time step chosen in the simulation and low-energy cut-off is due to the resolution of energy degradation of electrons as they traverse through the anode rod. Smaller time step will yield better energy resolution. It is important to choose a time step small enough to minimize such dependence for accurate calculation of the bremsstrahlung spectrum. Through the use of successively smaller time step, the electron distribution will gradually converge. In Fig. 9, we show the comparison of two electron

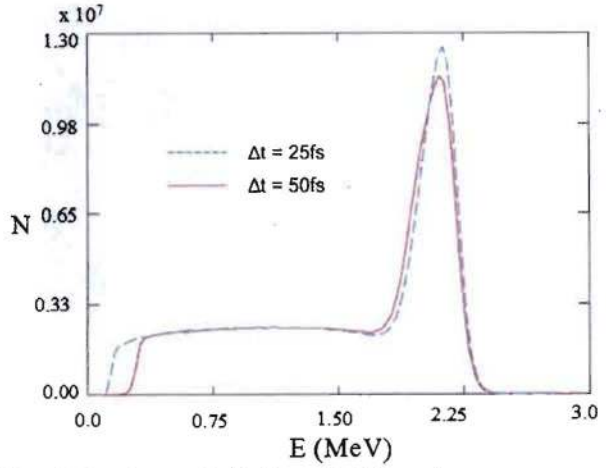

Figure 9.Two electron distributions with different time steps.

distributions resulting from time steps of 25fs and 50fs. It is evident that converged distribution has been achieved.The difference in the very-low energy cut-off is not important for radiographic applications because such low energy bremsstrahlung will not contribute to radiographic images. Consequently, we are confident that the choice of the time step of 50fs in our PIC simulation will give us the electron distribution with high fidelity. Using the methodology in the steady case, an electron phase space on the surface of the anode obtained from a 50-fs-time-step simulation is sourced into the MCNP computation for the bremsstrahlung spectrum.

D. MCNP Transport Calculations

To investigate the effects that the different PIC electron distributions would have on the diode X-ray spectra, each Merlin simulation case (steady-state, time dependent, and Monte Carlo) was linked with MCNP to obtain the bremsstrahlung spectrum. In this section, after briefly reviewing the MCNP calculation methodology, the results of the spectrum calculations will be reported and analyzed. In the approach to modeling Cygnus with the RCM, following the PIC calculations, the resulting electron distributions were linked directly into MCNP as an electron source. MCNP then calculated the electron transport, collisions, and the resulting X-ray emissions from the high Z anode/converter tip. Synthetic X-ray emissions were output as spectra only after the MCNP calculations had achieved excellent Monte-Carlo statistics. The results of the MCNP spectrum calculations are shown in the log-linear scaled plot in Fig. 10 where the area under the curves has been normalized to one. A so-called "best fit" spectrum, obtained by fitting experimental data from stepwedges, has been included on the spectrum plot for comparison.

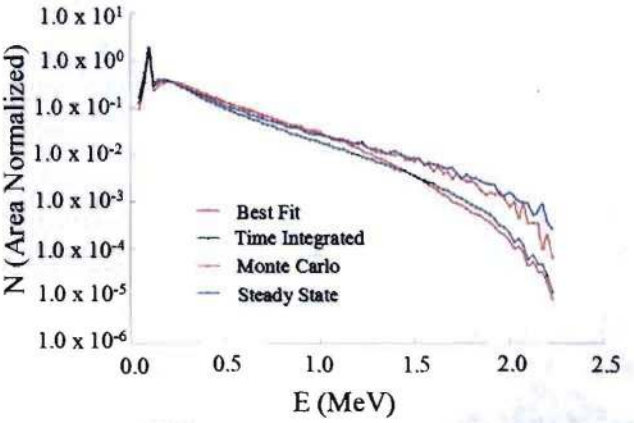

Figure 10. Gamma ray spectra calculated with the PIC electron distributions on a log-linear plot. The photon energy spectrum is independent of solid angle for cone angles less than six degrees from the axis of the anode where the vertex of the cone is the tip of the anode but its intensity attenuates according to spherical divergence (R^{-2} where R is radius from the tip of the anode).

A close examination of the synthetic spectra (Fig. 10) provides a basis for comparison and analysis. The spectra show three primary features: a characteristic line, the bremsstrahlung continuum, and the bremsstrahlung endpoint energy. Clearly visible in each spectrum is the 69.5 KeV K-edge of the tungsten anode. As expected, this K-edge intensity is higher than the continuum because the characteristic-line absorption and emissions are more efficient than the losses from bremsstrahlung during the electron collisions. The X-ray intensities in the continuum decrease as the x-ray energy increases. On the spectral graph (Fig. 10), between 0.5 MeV and 1.2 MeV, the slopes of the x-ray spectra are approximately linear (due to the logarithm scale) indicating the nearly exponential dependence of the intensity on energy. Above ~1.5

MeV, the spectral intensities attenuate rapidly with a downward inflection to the maximum energy 2.25 MeV, which was the end-point energy in the PIC simulations. The region of the spectra between 0.5 MeV and 1.2 MeV is important for analyzing the effects of the PIC electron distributions on the resulting diode spectra because the slope of the log-scaled spectrum is approximately linear, or $m=d(log(N))/dE$, where m is the slope, N is the spectral intensity and E is the X-ray energy. The magnitude of m is a figure of merit for the relative distribution of the x-ray energies within the spectrum. For example, for the time integrated spectrum, $m_{TI} \approx -1.4$ MeV^{-1} is lower than steady-state spectrum $m_{SS} \approx -1.2$ MeV^{-1} because it has a higher proportion of lower energy X-rays. In this case, the time-integrated spectrum is said to be "softer" than the steady-state spectrum.

Upon inspection of the PIC generated electron distributions, the explanation for the softness of the time-integrated spectrum is clear. The time-integrated electron distribution (Fig. 7) spans the energies from ~ 0.88 KeV to 2.25 MeV with a peak ~1.8 MeV and a Full Width at Half Maximum (FWHM) of about 1 MeV. In comparison, the steady-state PIC electron distribution (Fig. 5) has a relatively sharp peak at ~2.1 MeV and a FWHM of about 0.4 MeV.

Thus, a correlation exists between the mean and first moment of the source-electron distribution over energy and the spectral distribution of X-ray energies – i.e. the "hardness" or "softness" in the resulting bremsstrahlungspectra. In this case, the spectrum resulting from a given PIC electron source is a superposition of bremsstrahlung emissions from each electron collision, whose kinetic energy defines the bremsstrahlung endpoint. The relative contribution to the spectrum from electrons with a given energy is weighted intensity within the electron-energy distribution.

Comparisons with the Monte-Carlo spectrum reveal more about the correlations between the electron distributions and the resulting bremsstrhlung spectra. The Monte Carlo electron-energy distribution had a significant tail spanning the energies between ~0.30 MeV and ~2.0 MeV (Fig. 8) indicating the X-ray spectrum would be "softer" than the steady-state spectrum. But, the magnitude of the slope in the Monte-Carlo spectrum $m_{MC} \approx -1.2$ MeV^{-1}, is very close to the steady-state spectrum. This apparent hardness is due to the presence in the Monte-Carlo electron energy distribution of a narrow and tall peak whose average value was ~ 2.0 MeV and FWHM of ~0.4 MeV (which was from the converged case of the simulation with a sufficiently small time-step Δt shown in Fig. 8), similar to the peak in the steady state electron distribution.

When the spectra are plotted with a linear-linear scale (Fig. 11), a subtle difference between the Monte-Carlo and steady state spectra appears more evident. The distribution of steady-state x-rays between 0.5 MeV and 1.2 MeV is lower than the Monte-Carlo spectrum.

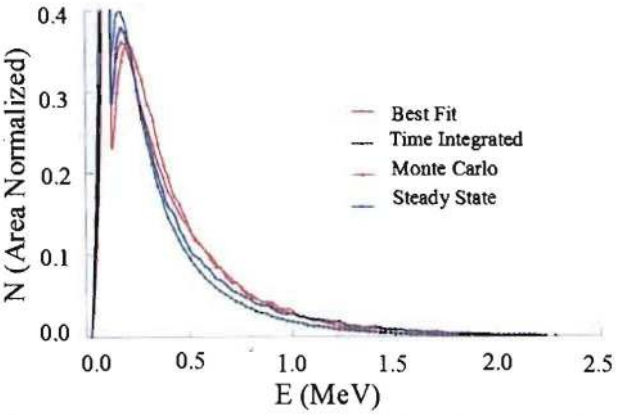

Figure 11. Gamma ray spectra calculated with the PIC electron distributions on a linear-linear plot.

This relative increase of the Monte-Carlo midrange X-rays is caused by the low energy tail in the source Monte-Carlo electron distribution. It is noted that, this relative increase in the Monte-Carlo spectrum agrees well with the best-fit spectrum between 0.5 MeV and 1.2 MeV.

In the spectra logarithm-plot (Fig. 10), the X-rays with energies above ~1.2 MeV appear to be significantly different but these variations are actually minor because, as seen with the linear scale (Fig. 11), the intensities of *all* the spectra appear to converge and overlap. This observation reinforces the importance of the region of the spectra between 0.5 MeV and 1.2 MeV for understanding the source spectra and its contributions to radiographic images.

III. Step-Wedge Transmission Calculations Compared with Experimental Data

To evaluate effects due to the differences in the calculated spectra and verify the results with data, calculations of the transmission curves of a tantalum (Ta) step-wedge were carried out.

A step-wedge is used to characterize an incident spectrum by filtering out portions of the spectrum in steps. The step-wedge is made with a set of blocks, usually of one material, with well-defined lengths. Stacked side by side and viewed normal to the transmission axis (Fig. 12), the

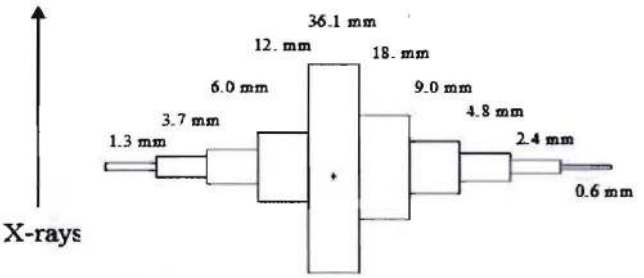

Figure 12. A Ta stepwedge used with Cygnus as modeled in MCNP. The height of each step is 9.0 mm and width 8.0 mm.

set of blocks resembles steps forming a wedge. The step lengths sample over a range of the material areal densities, which are obtained by multiplying the volume density of the

step-wedge material with the thickness of the step along the axis of X-ray transport.

Step-wedge transmission curves are obtained by plotting the x-ray transmission fraction T versus the areal density of each step. The transmission fraction is defined $T = n/n_0$, where n is the integrated intensity of the X-rays transmitted through the material and n_0 is the integrated intensity of the incident X-ray spectrum. In practice, the transmission fraction is obtained easily by measuring the x-ray flux with and without the step-wedge.

In this study, a set of simulations were calculated in order to verify the PIC electron distributions (steady-state, time dependent, and Monte Carlo) discussed in an earlier sections. These sources were used in MCNP calculations that included a full-geometry model of an experiment with Cygnus in which transmission data was collected with a Ta step-wedge (Fig. 12). The MCNP calculations were set-up to include the effects of X-rays scattered off objects within the solid-geometry model. Synthetic transmission curves were compared with step-wedge data from Cygnus in Fig. 13.. The "best-fit" source was also used to calculate a transmission curve.

A broad range of effects are evident in the low areal density region (< 25 g/cm^2) of the transmissions. These variations demonstrate the magnitude of sensitivity of the step-wedge transmissions to the subtle differences in the weighting of x-rays in the source spectra.

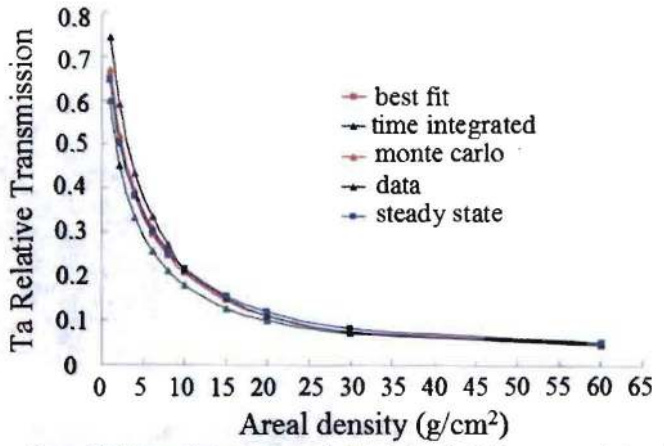

Figure 13. Transmission curves calculated with the PIC source models and a tantalum stepwedge object in MCNP are compared to Tantalum data collected with the Cygnus source.

Information is lost in the high-areal density (> 25 g/cm^2) region of the transmission plot (Fig. 13) where *all* the transmissions curves attenuate to roughly the same absolute transmission. The transmissions appear to attenuate because the X-ray transmissions have diminished below the system noise level, which was caused by scattered X-rays. The effects of scattered x-rays are implicit in the data but modeled explicitly in the MCNP simulations.

The differences in the steady-state, best-fit source, and the Monte Carlo spectra are hard to distinguish (Fig. 13) due to the small (few percent) relative differences in the X-ray spectra. However, the differences in the softness of the time integrated spectrum compared with the steady state spectrum are easily identified because $(m_{TI} - m_{SS})/ m_{SS} = .16$, i.e. the time-integrated spectrum is ~16% "softer" than the steady-state spectrum.

All of the transmission curves (Fig. 13) from the PIC calculated sources obtain noticeably lower transmission efficiencies than observed in the data for areal densities less than 15 g/cm^2. The lower transmissions suggest that the Cygnus model is consistently underestimating the "hardness" of the diode spectrum. Inclusion in the source model of features such as the tapered geometry of the anode and experimental waveform of the diode voltage in the Monte Carlo PIC simulations would further enhance the fidelity of the Cygnus spectrum and perhaps produce results closer to experimental data.

IV. Conclusion.

In summary, Cygnus spectrum has been calculated with increasing level of sophistication resulting in better comparison with data. The reflexing electrons through the anode needle have been shown to add important modification of the spectrum in the mid- to low-energy regions. To evaluate effects due to the differences of the spectra in the three simulation cases (steady-state, time dependent, and Monte Carlo), calculations of transmission curves of a Ta stepwedge were carried out. These transmission curves are generally lower than the data for low areal densities (< 25 g/cm^2). However, spectrum including the effects of reflexing electrons produces a transmission curve that agrees well with a best-fit case, which is the closest fit with the data to date. Inclusion of the tapered geometry of the anode and experimental waveform of the diode voltage would further enhance the fidelity of the Cygnus spectrum.

Acknowledgment

We thank the following for many useful technical discussions: Nicholas King, Todd Haines, Steve Lutz, and John Smith.

References

[1] Smith, John R., Carlson, R., Fulton, R. D., Altes, R., Carboni, V., Chavez, J. R., Corcoran, P., Coulter, W. L., Douglas, J., Droemer, D., Gibson, W. A., Helvin, T. B., Henderson, D. J., Johnson, D. L., Maenchen, J. E., Mitton, C. V., Molina, I., Nishimoto, H., Ormond, E. C., Ortega, P. A., Quicksilver, R. A., Ridlon, R. N., Rose, E. A., Scholfield, D. W., Smith, J., Valerio, A. R., White, R. T. A. Mehlhorn (ed.), "Performance of the Cygnus X-ray Source," Beams 2002: *14th International Conference on High-Power Particle Beams*, Albuquerque, New Mexico, June 23–28, 2002. **650**, 135–8.

[2] Weidenheimer, D., Corcoran, P., Altes, R., Douglas, J., Nishimoto, H., Smith, I., Stevens, R., Johnson, D. L., White, R., Gustwiller, J., Maenchen, J. E., Menge, P., Carlson, R., Fulton, R. D., Cooperstein, G., Hunt, E. "Design of a driver for the Cygnus X-ray source," *Proceedings of the 13th IEEE International Pulsed Power Conference, Digest of Technical Papers*, Las Vegas, NV, June 17–22, 2001, **1**, 591–5.

[3] Kwan, Thomas J. T., Mathews, Allen R., Christenson, Peggy J., and Snell, Charles M., "Integrated system simulation in X-ray radiography," *Comp. Phys. Comm.* **142**, 263 (2001).

[4] Kwan, Thomas J. T., and Snell, C. M., "Methods of Monte Carlo electron transport in particle-in-cell codes." In R. Alcouffe, R. Dautray, A. Forster, G. Ledanois, B. Mercier (eds.), *Monte Carlo Methods and Applications in Neutronics, Photonics, and Statistical Physics: Proceedings (Lecture Notes in Physics, Vol. 240)* (Springer Verlag, New York, 1985).

[5] X-5 Monte Carlo Team, MCNP, *A General Monte Carlo N-Particle Transport Code, Version 5*, Los Alamos National Laboratory, Los Alamos, NM, LA-UR-03-1987 (2003).

[6] Cooperstein, G; Boller, J. R.; Commisso, R. J.; Hinshelwood, D. D.; Mosher, D.; Ottinger, P. F.; Schumer, J. W.; Stephanakis, S. J.; Swanekamp, S. B.; Weber, B. V., "Theoretical modeling and experimental characterization of a rod-pinch diode," *Phys. Plasmas*, **8**, 4618 (2001).

[7] Mahaffey, R. A., Golden, J., Goldstein, S. A., and Cooperstein, G., "Intense electron-beam pinch formation and propagation in rod pinch diodes," *Appl. Phys. Lett.*, **33**, 795 (1978).

[8] Lin Yin, Kevin Bowers, R. Carlson, B. G. DeVolder, Thomas Kwan, J. R. Smith, C. M. Snell,M. J. Berninger , "Electron Dynamics of the Rod-Pinch Diode in the Cygnus Experiment at Los Alamos," *Proceedings of the 2005 Particle Accelerator Conference, Knoxville Tn. IEEE Catalog Number 05CH37623C ISBN 0-7803-8860-7*